

Effects of stratification and charge cooling on combustion in a gasoline direct-injection compression ignition (GDCI) engine

Haiwen Ge¹, Peng Zhao^{2*}

¹Department of Mechanical Engineering, Texas Tech University, Lubbock, TX, USA 79409

² Department of Mechanical, Aerospace & Biomedical Engineering, UT Space Institute, University of
Tennessee, Knoxville, Tennessee 37388

* **Correspondence:** pzhaol2@utk.edu

Abstract

With the development of low temperature engine combustion strategies, performance of gasoline-type fuels under compression ignition conditions has attracted extensive research interest. Meanwhile, for the sake of co-optimization of engines and fuels for future ground transportation, identification and evaluation of general fuel properties should be a core research priority instead of endless testing of specific fuels. In this study, the roles of fuel octane sensitivity in characterizing the ignition performance of gasoline surrogates have been systematically investigated under typical gasoline direct ignition compression ignition (GDCI) engine conditions using 3D combustion CFD simulation, especially considering the subsequent in-cylinder charge stratification and charge cooling. Two different operating conditions, high boost pressure low boost temperature (beyond-RON) case and low boost pressure high boost temperature (beyond-MON) case, were considered. By comparing with our previous zero-dimensional chemical kinetic study of gasoline surrogates in advanced compression ignition (ACI) engines (Tao et al., 2018),

the effects of stratification and charge cooling on the combustion processes are investigated. It is found that different fuel octane sensitivities lead to slight difference in equivalence ratio stratification and charge cooling due to differences in volatility. However, fuel reactivity is still the more dominant factor than the stratification and charge cooling effects in determining combustion phasing. The present results help to justify the P-T domain framework for engine autoignition analysis of overlapping pressure-temperature trajectory with ignition delay iso-contour. The results also provide useful guidance to the understanding of GCI combustion process, and to the evaluation of controlling fuel properties and the selection of alternative fuels in GCI engines.

Keywords: gasoline direct-injection compression ignition (GDCI), low temperature combustion, octane sensitivity, ϕ -sensitivity, stratification, charge cooling, toluene reference fuel (TRF)

1. Introduction

Due to advantages of low cost, high durability and capability to utilize high energy density liquid fuels, internal combustion engines equipped with advanced combustion strategies are expected to continue playing a critical role in transportation decarbonization. In the past few decades, advanced compression ignition (ACI) engines featured by diesel-like efficiency and low emissions have been developed to incorporate the advantages of both conventional spark-ignition (SI) and compression ignition (CI) engines, such as homogeneous charge compression ignition (HCCI), premixed charge compression ignition (PCCI), reactivity controlled compression ignition (RCCI), etc.¹ These novel combustion strategies largely rely on the compression ignition of homogeneous or moderately stratified fuel/air mixtures under dilute conditions, such that in-cylinder regions with fuel-rich mixture and high peak temperatures can be avoided and the engine

can operate in the low temperature combustion (LTC) regime. Among these combustion strategies, GDCI is a very attractive PCCI technology including multiple combustion modes (i.e., PPCI or HCCI, even MCCI), where LTC can be achieved by direct injection of conventional gasoline, a fuel with relatively long ignition delay and high volatility. Injection timing is a primary knob to control the extent of fuel-air mixing and subsequent in-cylinder charge stratification, and eventually combustion is triggered by the autoignition of local fuel-air mixture with the most favorable equivalence ratio and temperature. Consequently, properly designed GDCI requires minimal modification to the existing engine architecture and fuel supply infrastructure, and allows sufficient time for fuel-air mixing, high compression ratio, as well as relatively low soot and NO_x emission.

The GDCI concept is proposed by Kalghatgi, and since then has raised extensive research effort among industry, academic institutions and national labs.^{2, 3} Delphi is leading the development of GDCI enabled engine technology.⁴⁻¹¹ Aramco's research of GDCI focused more on the effects of fuel properties.¹²⁻¹⁷ Extensive studies on GDCI have been conducted by the University of Wisconsin-Madison,¹⁸⁻²² Lund University,²³⁻²⁸ Argonne National Lab,²⁹⁻³³ and University of New South Wales.³⁴⁻³⁷ The developments of GDCI technology before 2018 have been well summarized.³⁸ Fuel properties, particularly the fuel reactivity, distillation property, and octane sensitivity, are critical for the combustion and emission of the GDCI engines, and hence have been a major focus of these studies. For example, Aramco tested conventional gasoline and lower RON gasoline fuels on a GDCI engine and founded that high reactivity gasoline with a RON close to 60 produces much lower soot emissions than the conventional mixing-controlled diesel combustion.¹⁶ Dempsey et al. used 3D engine CFD to provide an overview of GDCI combustion

processes under different stratification levels, including partial, moderate and heavy fuel stratifications.³⁹

Depending on the specific operating strategies, GDCI can be realized under different conditions (i.e., beyond RON and beyond MON). For GDCI equipped with cooled external EGR with boosted intake pressure, the engine operates under beyond RON conditions; while GDCI realized by trapping hot residuals from negative valve overlapping (NVO) operates under beyond MON conditions with elevated intake temperature. Regardless which operating condition, kinetic behavior of gasoline under compression conditions is fundamentally important and has received extensive research interest. Previous work⁴⁰ conducted kinetic investigation on the manifestation of octane rating and sensitivity of various gasoline surrogates under representative compression ignition conditions and demonstrate such effects using a pressure-temperature framework, as an extension of the Livengood-Wu integral analysis.⁴¹ The role of conventional fuel metrics such as octane rating and octane sensitivity has been found to be substantially different in different engine operating regimes, i.e., beyond RON and beyond MON conditions. Their results are intriguing but are solely based on thermodynamics and chemical kinetics. In actual GDCI engines, there are two dominant processes associated with the injection that must be considered to fully understand GDCI combustion. The first factor is charge stratification, which meanwhile allows exploiting the ϕ -sensitivity of the fuel - the change in ignition delay time (IDT) with respect to the change in fuel-to-air equivalence ratio (ϕ). Besides the inherent influence from fuel molecular structure,⁴² recent work has suggested that fuels with high ϕ -sensitivity frequently exhibit strong negative-temperature coefficient (NTC) and are associated with pronounced low temperature fuel chemistry.⁴³ For gasoline fuels whose reactivity can be adequately described by surrogates such as toluene primary reference fuel (TPRF), a high ϕ -sensitivity actually requires a lower octane

sensitivity (S) and the fuel is hence closer to the primary reference fuels (PRF). Therefore, it can be conjectured that the reactivity of gasoline with lower octane sensitivity has stronger dependence on in-cylinder stratification, and exhibits greater ignition timing variation in GDCI combustion. The second factor that should be accounted for is the charge cooling effect, which is especially important for gasoline with strong NTC behavior, whose chemical reactivity exhibits non-monotonic dependence on charge temperature. As the mixture temperature drops due to vaporization, the trajectory of a charge pocket in the pressure-temperature domain is highly possible to bend into the NTC or the low temperature regime, leading to non-monotonicity in reactivity.⁴⁴

Without devaluing the usefulness of 0D engine autoignition analysis combining fuel ignition delay and engine thermodynamic trajectory, the objective of the current work is to further investigate the 3D effects of stratification and charge cooling on GDCI combustion, and understand the complex role of critical fuel properties such as octane sensitivity and ϕ –sensitivity played in GDCI combustion. The engine thermodynamic conditions are selected from the previous 0D kinetic study of fuel metric under ACI conditions along the combustion phasing iso-contour.^{40, 41, 45} Detailed in-cylinder flow, spray dynamics and mixing are systematically considered in the current computational study. The results are further compared with the 0D kinetic study without considering stratification and charge cooling. This work aims to provide useful guidance for GDCI fuel screening and combustion optimization.

2. Model and validation

The present study employs a typical diesel engine configuration that has the same bore and stroke as a GM 1.9 L in-line four-cylinder diesel engine with intake valve closing (IVC) is at -149 degrees ATDC and exhaust valve opening (EVO) is at 130 degrees ATDC. Table 1 shows the

engine specification. The piston bowl shape is adopted from the optimized one from previous work.⁴⁶ A commercial finite volume computational fluid dynamics program CONVERGE™ is employed to simulate the fuel injection and combustion processes of a gasoline direct-injection compression ignition engine.⁴⁷ The same spray and combustion models as the previous research⁴⁸ were employed, including the real fluid model described by the Redwich-Kwong equation of state and the SAGE combustion model. Adaptive zoning is activated to speed up chemistry calculation. All the simulations use unsteady RANS with RNG $k - \varepsilon$ model.⁴⁹ Constant diffusivity coefficients were assumed, with turbulent Prandtl number of 0.9 and turbulent Schmidt number of 0.78. Kelvin-Helmholtz Rayleigh-Taylor (KH-RT) breakup model is used for spray dynamics.⁵⁰ Discharge coefficient is set to 0.9. Rebound/slide model is employed for spray wall interaction. No-Time-Counter collision model is used for droplet interaction. Drag effects are considered using the dynamic drop drag model, with the O'Rourke turbulent dispersion model.⁵¹ Droplet evaporation is described using the Frössling model.⁵² Uniform distribution is applied to the initial size of droplets. A top-hat injection profile is adopted. The simulations start from IVC and end at EVO.

Table 1: engine specifications

Bore (mm)	82
Stroke (mm)	90.4
Connecting rod (mm)	145.4
Engine speed (rpm)	1000
Compression ratio	17:1
Injection pressure (bar)	800
Injection duration (degrees)	4.2
Nozzle hole number (-)	7
Nozzle hole diameter (mm)	0.141
Swirl ratio (-)	0

The choice of surrogate model of gasoline and the chemical mechanism follows the authors' earlier work.⁴⁰ Specifically, a robust TRF surrogate model is adopted to model the practical

gasoline, which has been demonstrated with good performance in capturing measured knock onset for a wide range of SI experiments.⁵³ With this surrogate model, the composition of TPRF gasoline can be determined (as shown in Table 1) to match the required fuel metrics. It has been shown that the Andrae TRF mechanism shows lower relative error to predict measured ignition delay and flame speed in a wide range of thermodynamic conditions than the other available mechanisms.⁵⁴ A thorough validation of Andrae mechanism is performed against isooctane kinetic targets collected in the literature, with satisfactory performance⁵⁵

The combustion chamber of the engine is represented by a sector mesh as shown in Figure 1 (a). Adaptive mesh refinement (AMR) and fixed embedding were used to balance computational efficiency and accuracy. Base mesh size is set to 1 mm. Three level embedding based on temperature and velocity was applied to AMR. Thus, the smallest grid size is 0.125 mm, which is more refined than the recommended setup from Kodavasal et al.²⁹ but coarser than ECN's setup⁵⁶. The base mesh size (1 mm) is further confirmed based on the grid convergence study. As shown in Figure 1 (b), the pressure histories of three different base mesh sizes (2 mm, 1 mm, 0.8 mm) for a typical case at injection timing -10 degrees ATDC largely overlap and have demonstrated satisfactory grid independence.

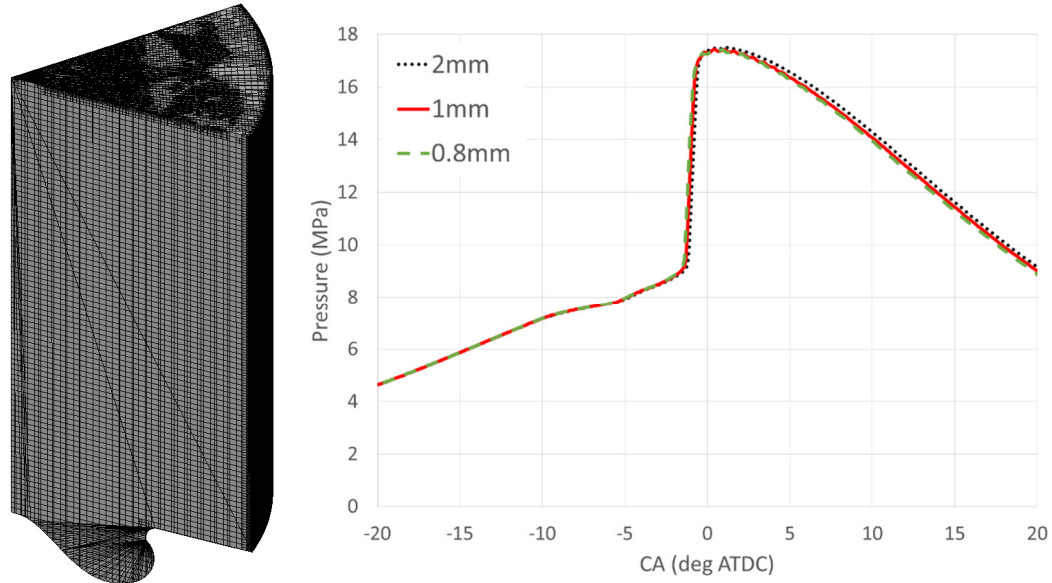


Figure 1: (a) sector mesh used in the simulation and (b) grid convergence for a typical case.

The spray model is firstly validated in an evaporating non-reactive spray of the ECN Spray G. ⁵⁶

The initial temperature and pressure of the constant-volume combustion vessel are 573K and 60 bar. The initial mixture in the combustion vessel consists of 6.52% CO₂, 3.77% H₂O, and 89.71% N₂ in mass fraction. Figure 2 shows the comparison of measured and predicted liquid penetrations.

The average values and standard deviations of the liquid penetrations are evaluated from the data of the eight spray plumes. Good agreement is achieved, which implies that the present spray model is reliable.

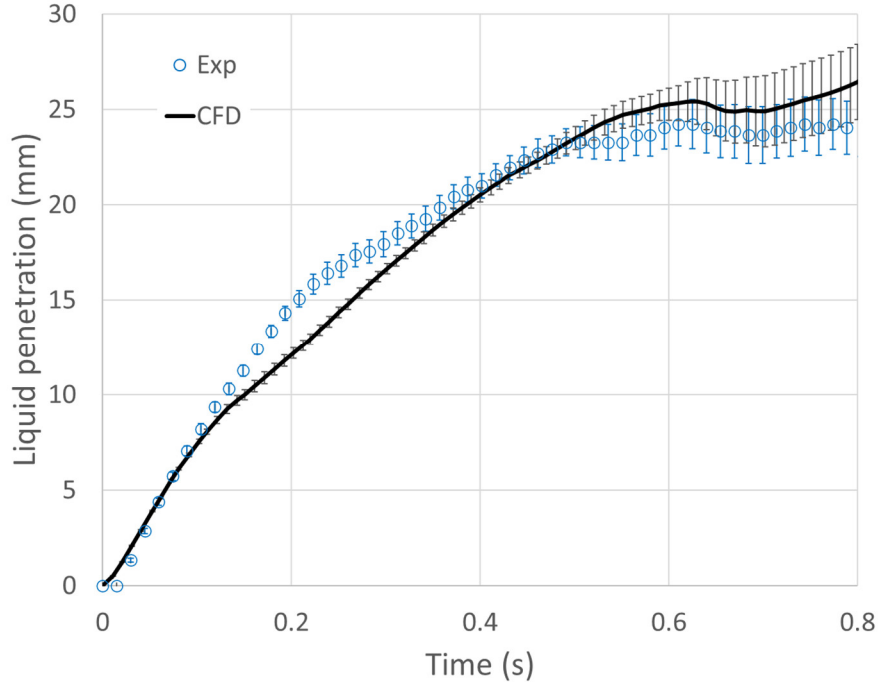


Figure 2: measured and predicted liquid penetrations.

3. Results and Discussion

3.1 Kinetic manifestation of octane sensitivity and ϕ sensitivity of TRFs

Figure 3 shows the homogeneous adiabatic constant volume ignition delay time of different TRFs with the same RON but different S values in a broad range of temperatures and pressures at the same equivalence ratio, $\phi = 0.3$. A direct observation is that all the TRFs exhibit very similar high temperature ignition delay (i.e., temperature beyond the upper turnover state of the NTC regime) with Arrhenius behavior, while the major deviations in ignition delay time are seen in the low and intermediate temperature regimes affected by the low temperature chemistry, which is directly related to their differences in fuel sensitivity. Another observation is that with increasing octane sensitivity, the non-monotonicity in the ignition delay time due to the NTC effect is gradually eliminated for a given pressure, which consequently leads to elongated ignition delay time under low to intermediate temperatures for high sensitivity TRFs. These observations are consistent with the earlier findings by Leppard, where the chemical origin of octane sensitivity of different classes of hydrocarbons is found to correlate to their different extent of NTC.⁵⁷ The

observations here have useful insights in that the ignition delay map of gasoline is primarily controlled by the S value of the TRF fuel, with lower octane sensitivity fuels exhibiting stronger similarity to PRF fuels and more pronounced NTC behavior.

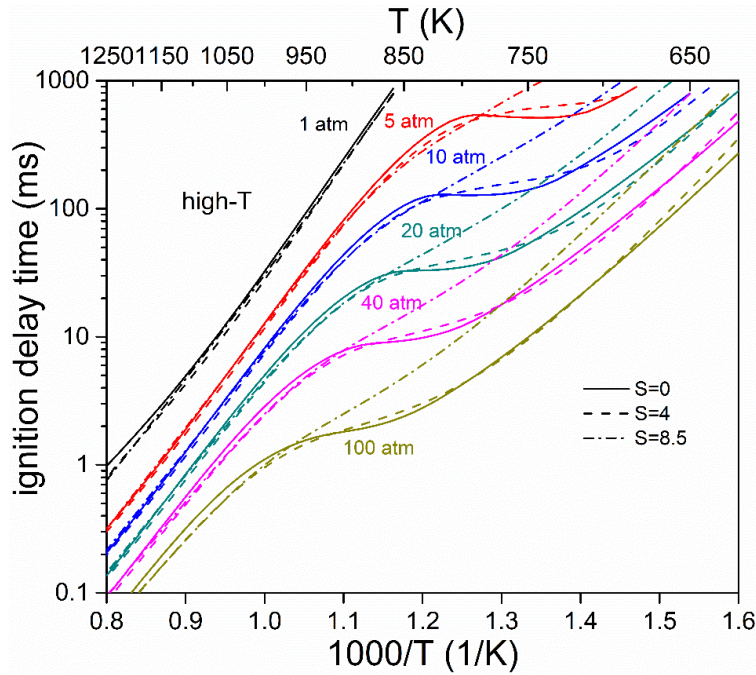


Figure 3: Adiabatic constant volume ignition delay time of TRFs with matched RON=96.8 but different S values, $\phi = 0.3$ in air.

A key fuel property for actual GDCI combustion is the ϕ sensitivity, which characterizes the dependence of ignition delay on charge equivalence ratio. Figure 4 shows the constant volume, adiabatic ignition delays of TRFs with strong and weak octane sensitivity as a function of mixture equivalence ratio. In the intermediate to high temperature regime, i.e., 900K and beyond, the ignition delay time of both TRFs exhibit slight changes for mixture from lean to stoichiometric, with nearly fixed activation energy. Hence, it can be expected that for engine thermodynamic trajectories crossing this regime, the corresponding combustion phasing will have limited sensitivity to different extent of in-cylinder charge stratification induced by injection timing. While in the low to intermediate temperature conditions, ignition delay can be reduced by half to one

order of magnitude for both fuels from lean to stoichiometric, indicating stronger dependence of combustion phasing on charge stratification. Accordingly, the PRF has shown more pronounced NTC behavior approaching stoichiometry. We shall see in the following how the actual GDCI combustion depends on the ϕ sensitivity.

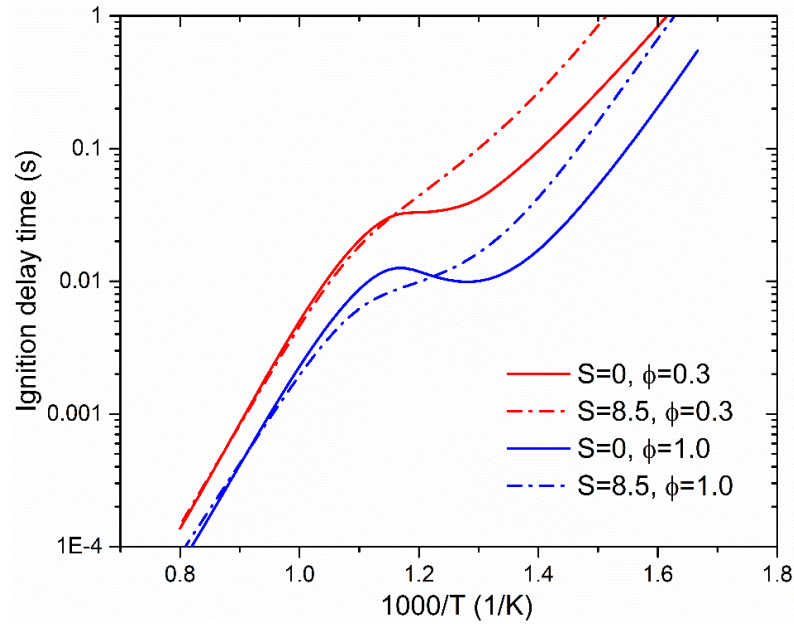


Figure 4: Adiabatic constant volume ignition delay time of TRFs with matched RON=96.8 but different S values at 20 atm, with different equivalence ratios in air.

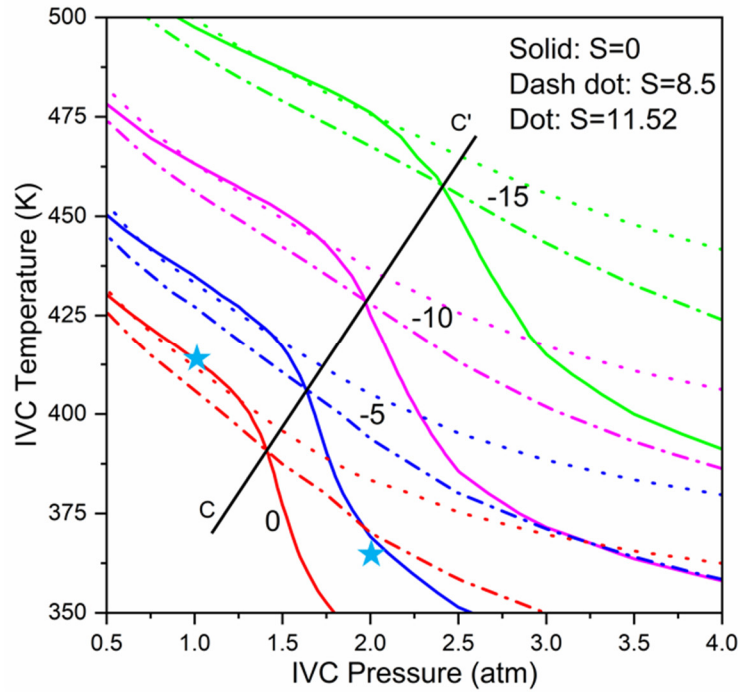


Figure 5: Calculated CA10 iso-contours in 0-D HCCI combustion of TRFs with matched RON=96.8 but different S values, $\phi = 0.3$ in air

Based on the dependence of TRF ignition delay time on octane sensitivity under different thermodynamic conditions, Figure 5 further shows the CA10 iso-contour of TRFs with different octane sensitivity for 0-D HCCI combustion simulations without considering vaporization cooling under different IVC thermodynamic conditions. A perfectly mixed fuel/air mixture is introduced at IVC instant of -142° ATDC. A good indicator of ignition delay CA10 is utilized to mark the instant when 10% of fuel is burnt. Clearly, in the low-pressure high-temperature beyond-RON conditions (above the cutting line CC'), CA10 iso-contours largely overlap for TRFs with different octane sensitivity; while in the high-pressure low-temperature beyond-MON conditions, CA10 substantially advances for TRFs with low octane sensitivity, regardless the same RON.

Table 2: fuel mole fraction, octane rating, octane sensitivity and IVC thermodynamic conditions of each case.

Case #	S	RON	n-heptane (%)	iso-octane (%)	Toluene (%)	Pressure (bar)	Temperature (K)
1	0	96.8	1.85	98.15	0	2	365
2	4	96.8	6.52	65.05	28.43	2	365
3	8.5	96.8	11.94	27.65	60.41	2	365
4	0	96.8	1.85	98.15	0	1	415
5	4	96.8	6.52	65.05	28.43	1	415
6	8.5	96.8	11.94	27.65	60.41	1	415

With the kinetic insights obtained from the 0D autoignition and HCCI conditions, a simulation matrix of GDCI combustion is designed as shown in Table 2, including fuel sensitivity, RON, composition (in mole fraction), IVC pressure and temperature. A RON value of 96.8 is kept as the same for all the cases. The octane sensitivity of the fuel varies from 0 (i.e., PRF) to 8.5 (TRF with 60.4% toluene by mole). Cases 1-3 correspond to a beyond-RON case with a high-pressure low-temperature boosting conditions, while cases 4-6 represent a beyond-MON case with a low-pressure high-temperature boosting conditions. For each case, a sweep in SOI (start of injection timing) is conducted, including (a) -40; (b) -30; (c) -20; (d) -10 degrees ATDC. For all the cases, the global equivalence ratios are kept as 0.3. For all 0-D simulations, a perfectly mixed fuel/air mixture is initialized at the corresponding SOI, such that the 0-D simulation results only reflect the chemical kinetic effects.

3.2 Comparison of 0D and 3D simulation of GDCI combustion

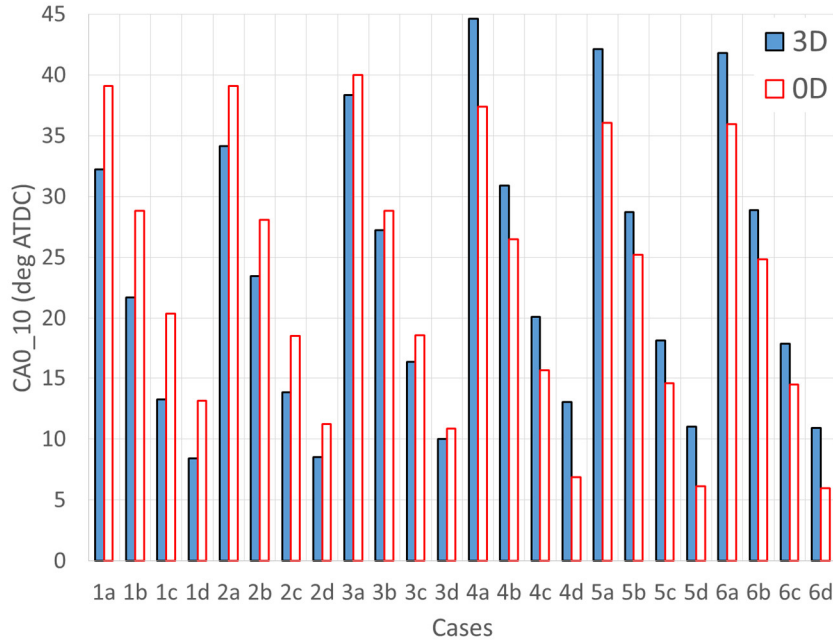


Figure 6: Comparison of CA0_10 between 0D and 3D CFD simulations of all cases.

In this section, the results of 0D and 3D CFD simulations are compared. Chemkin-Pro was used for the 0D HCCI simulation. Comparing to the 0D simulations, the 3D simulation additionally considers fuel injection and the consequent liquid fuel evaporation and mixing with the air. This leads to stratification and charge cooling that may influence the ignition and combustion processes. Since the global equivalence ratio is below unity, the in-cylinder stratification will always lead to shorter ignition delay than the perfectly mixed lean mixture as being considered in 0D simulation. Although charge cooling always tends to decrease the charge temperature, it does not necessarily always postpone the ignition delay. From Figure 3, it is straightforward to see that under either very high or very low temperature conditions, the reduced charge temperature always tends to decrease the temperature and leads to longer ignition delay, thereby competing with the stratification effects. While under intermediate to high temperature conditions, it is possible that

charge cooling can reduce the temperature below the NTC upper turnover state, and lead to a thermodynamic trajectory passing through the NTC regime, where a lower temperature eventually leads to reduced ignition delay. Under such conditions, the charge cooling effect can hence have synergy with the stratification to substantially advance ignition.

For all the GDCI simulation, CA0_10 is used to indicate ignition delay, which is defined as the period between SOI and the moment when 10% of fuel is burnt. Figure 6 shows the comparison of CA0_10 between 0D and 3D CFD simulations for all cases. Both 0D and 3D simulations show the same trend with respect to the injection timing. When the injection timing is retarded, the in-cylinder pressure and temperature are higher than the early injection cases, which results in much shorter ignition delay. It can be observed that for the beyond-RON Cases 1-3, 3D simulations predict much shorter ignition delay than the 0D simulations, regardless fuel and injection timing. This is well expected since in-cylinder charge stratification in the 3D cases creates stoichiometric and richer regions, which always tend to facilitate ignition, leading to consistently faster ignition compared with the corresponding perfectly mixed 0D cases. The charge cooling effects are either not dominant or exhibit synergy with the stratification effects. However, comparison for the beyond-MON Cases 4-6 shows the opposite trend, where CA0_10 predicted by 3D CFD simulations is longer than that predicted by the 0D CFD simulations, implying slower ignition in the 3D case. This must be due to the charge cooling effects. The beyond-MON cases have low-pressure high-temperature boosting conditions, with which the charge cooling effects are more evident and become more dominant than the stratification effects. The comparison in Figure 6 then demonstrate that stratification and charge cooling may lead to either synergistic or competing effects when couple with thermal chemistry, which can either facilitate or postpone GDCI ignition delay depending on the engine operating conditions.

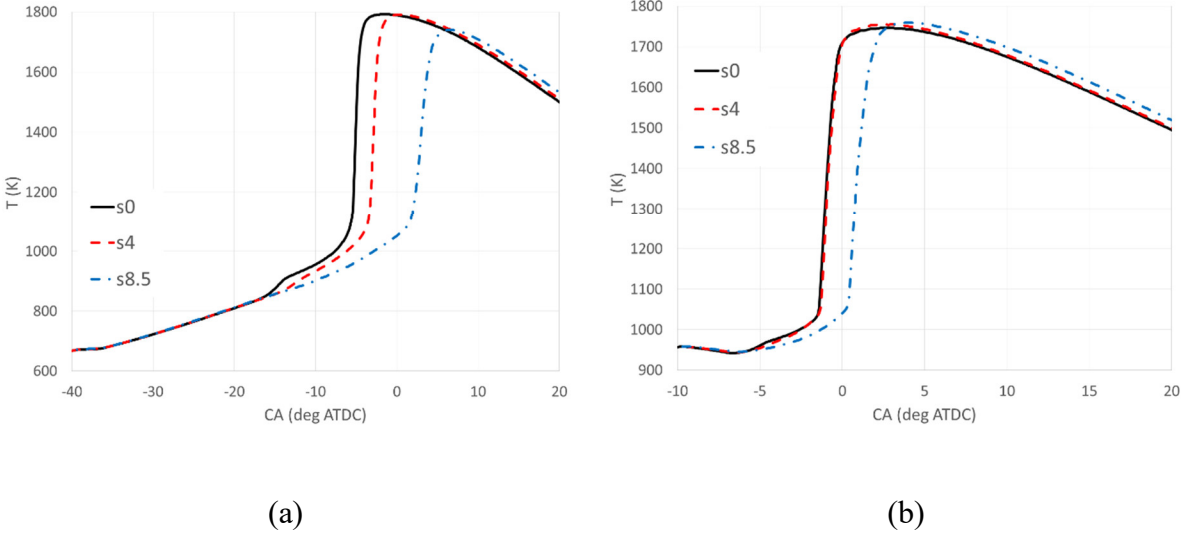


Figure 7: Comparisons of averaged in-cylinder temperature between different fuel sensitivities: $SOI = -40$ (a) and -10 (b) degree ATDC for 3-D CFD results of the beyond-RON Cases 1-3.

Figure 7 shows the comparisons of averaged in-cylinder temperature of 3D CFD simulations for different octane sensitivities ($S=0, 4, 8.5$) of Cases 1-3 that are under the beyond-RON condition. The left plot is for $SOI = -40$ degrees ATDC and the right one is for $SOI = -10$ degrees ATDC. For the early injection cases, more obvious low-temperature heat release is observed for fuels with lower octane sensitivity, which is consistent with the kinetic analysis of TRFs under HCCI conditions. Compared to the high octane sensitivity fuel, the PRF fuel with zero sensitivity can elevate the mean temperature by at least 50 K. In the late injection case, obvious charge cooling is observed from the reduced mean temperature right before -5 CA ATDC. For both early and late injection cases, no evident difference in temperature before the ignition is observed between different fuel octane sensitivities for both early injection and late injection cases. It implies that the cooling effects are about the same with different fuel compositions.

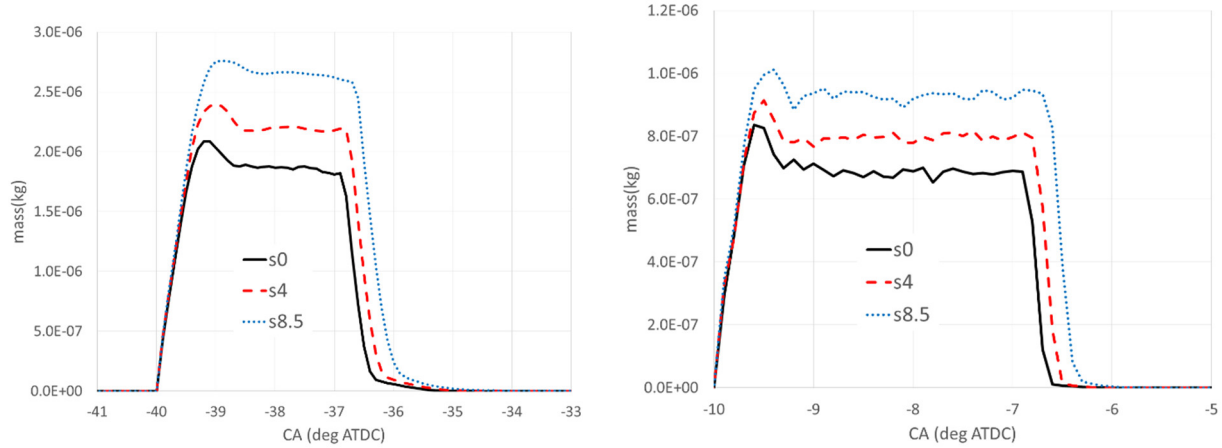


Figure 8: Total liquid fuel in cylinder for SOI=-40 (left) and -10 (right) degrees ATDC of the beyond-RON Cases 1-3 ($p_{boost} = 2 \text{ bar}$; $T_{boost} = 365 \text{ K}$).

To further investigate the effects of physical and chemical properties of the surrogate fuel models, in-cylinder total liquid fuel mass, averaged equivalence ratio and its variance are compared for Cases 1-3. Figure 8 shows the profiles of total liquid mass in cylinder for SOI=-40 and -10 degrees ATDC of Cases 1-3, which have the boost pressure of 2 bar and boost temperature of 365 K . It can be seen that the different surrogate fuels have different volatilities. The one with higher fuel octane sensitivity has higher concentration of toluene and thus has lower volatility that leads to lower evaporation rate. Thus, it has relatively more liquid fuel left and takes more time to completely vaporize into gaseous fuel. Nevertheless, for the early injection cases, it takes about 5 degrees of crank angle for all the liquid fuel to vaporize into gaseous fuel, which is much shorter than the ignition delay (32~39 degrees, c.f., Figure 5). Thus, the fuel injection, evaporation, and mixing processes have negligible impacts on the ignition and combustion processes. For the late injection cases, it takes about 3.5 to 4 degrees of crank angle, which is close to the ignition delay (8~9 degrees, c.f., Figure 5). Therefore, there is a good chance that the fuel evaporation occurs simultaneously with the evident chemical reactions. Their interactions hence cannot be neglected.

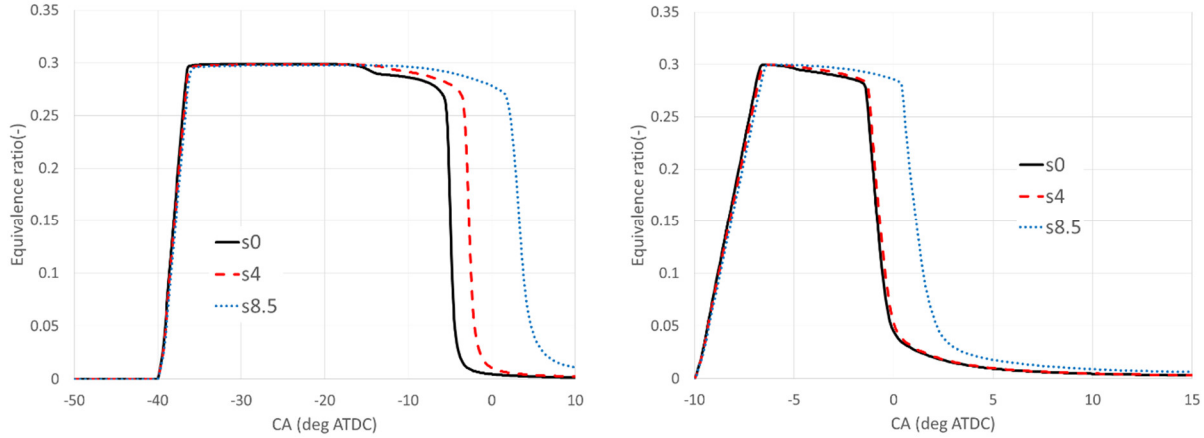


Figure 9: In-cylinder-averaged equivalence ratio for SOI=-40 (left) and -10 (right) degrees ATDC of the beyond-RON Cases 1-3 ($p_{boost} = 2 \text{ bar}$; $T_{boost} = 365 \text{ K}$).

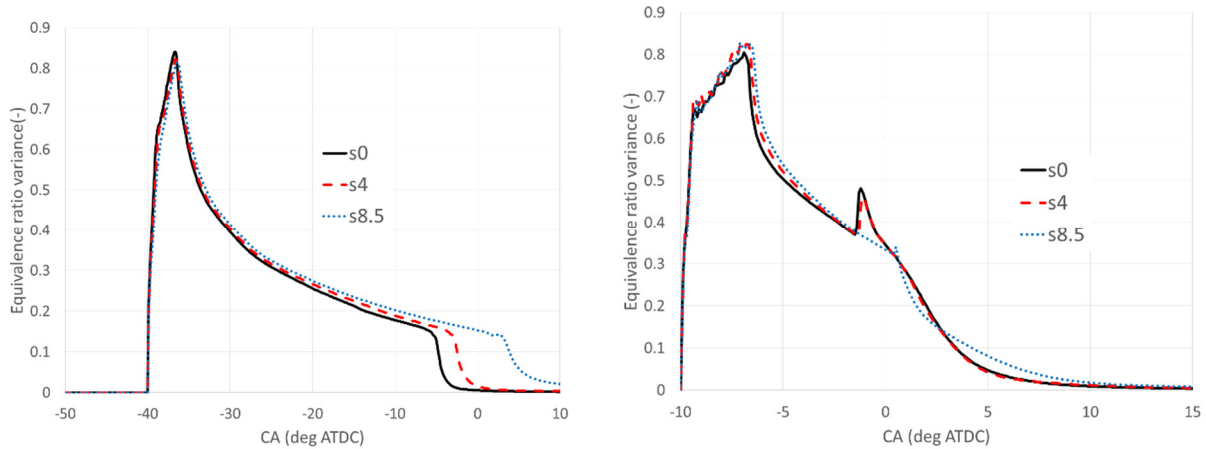
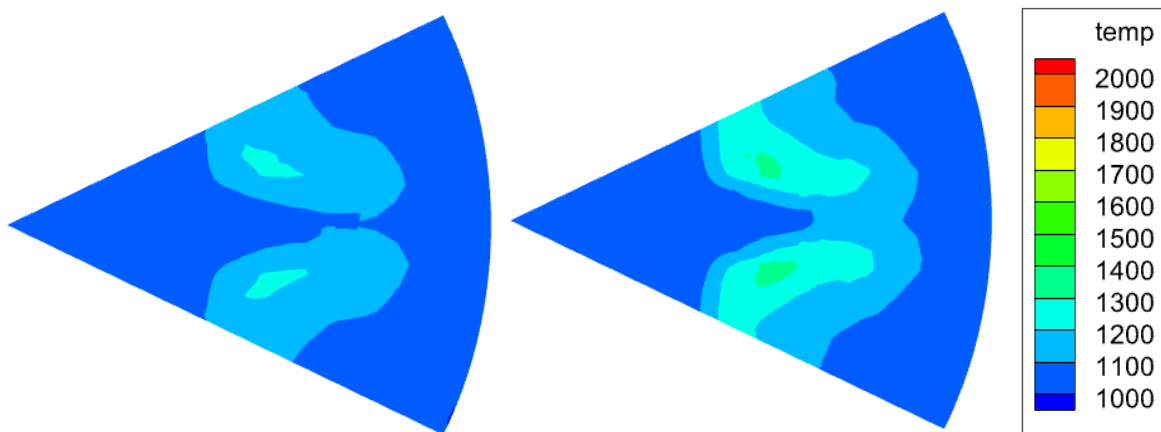


Figure 10: Variance of in-cylinder equivalence ratio for SOI=-40 (left) and -10 (right) degrees ATDC of the beyond-RON Cases 1-3 ($p_{boost} = 2 \text{ bar}$; $T_{boost} = 365 \text{ K}$).

Figure 9 shows the profiles of in-cylinder mass-weighted averaged equivalence ratio for SOI=-40 and -10 degrees ATDC of Cases 1-3. For the early injection case (left), the equivalence ratio reaches its maximum (0.3) around -36 degrees ATDC for different fuel sensitivity. After that, it plateaus until -16 degrees ATDC. For the PRF model ($S=0$), its equivalence ratio starts to decrease at -17 degrees ATDC, which indicates that the chemical reaction starts to consume the fuel. For the fuels with higher sensitivity, their equivalence ratios start to decrease later, which implies the longer ignition delay. For the late injection case (right), the plateau period is much shorter: only

1~2 degrees. Figure 10 shows the profiles of variance of in-cylinder equivalence ratio for SOI=-40 (left) and -10 (right) degrees ATDC of Cases 1-3. The variance indicates the level of inhomogeneity of the mixture (stratification). Higher variance indicates higher inhomogeneity of the mixture (stronger stratification). After the end of injection and before combustion, higher fuel octane sensitivity case has higher variance of equivalence ratio. This is due to its slower evaporation rate that slows down the consequent mixing process. For the present cases that have global lean mixture, high variance of equivalence ratio usually benefits faster combustion, since it implies more mixture that is close to stoichiometric. However, the kinetic results in Figure 5 show that higher fuel sensitivity leads to slower ignition under beyond-RON conditions. Thus, it can be concluded that the difference in stratification with different fuel sensitivity is not the reason of their different combustion behaviors. It should be due to their differences in chemical kinetics.



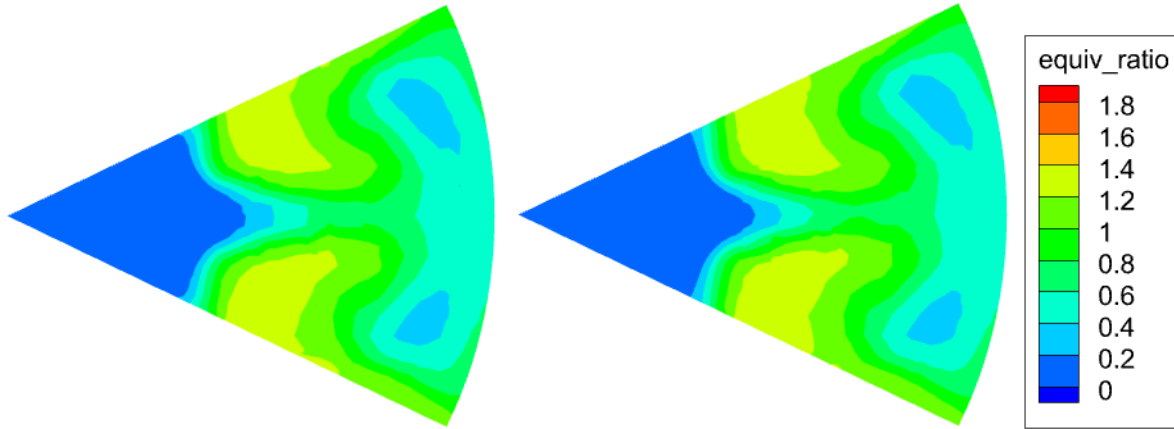


Figure 11: temperature (top) and equivalence ratio (bottom) distribution before and after ignition (Case 1; SOI=-10 degrees ATDC): CA= -1.47 (left) and -1.37 (right) degrees ATDC.

Figure 11 shows the temperature and equivalence ratio distribution before (CA=-1.47 degrees, ATDC, left) and after ignition (CA=-1.37 degree ATDC, right) of Case 1 ($p_{boost} = 2 \text{ bar}$; $T_{boost} = 365 \text{ K}$; $\text{fuel sensitivity} = 0$) and SOI=-10 degrees ATDC. The top row shows temperature distribution while the bottom row includes equivalence ratio. For each row, the left column implies the instant before ignition while the right column is after ignition. Before the ignition, slightly high temperature around 1300K is observed on the wing of the spray plume, which is due to the heat release from the low temperature combustion. The distribution of equivalence ratio indicates heavy fuel stratification, which shows rich mixture near the wings of the spray plume and the ignition spots have an equivalence ratio of about 1.4. The flame shape shows a W-shape in top view, which correlates with the spray plume and the consequent fuel vapor distribution. The W-shape flame reflects the influence of the fuel injection that generates the fuel stratification on the combustion process. Therefore, the results in Figure 11 are associated with low-temperature heat release, rich ignition kernel, and relatively strong stratification, representing a typical PPCI combustion mode.

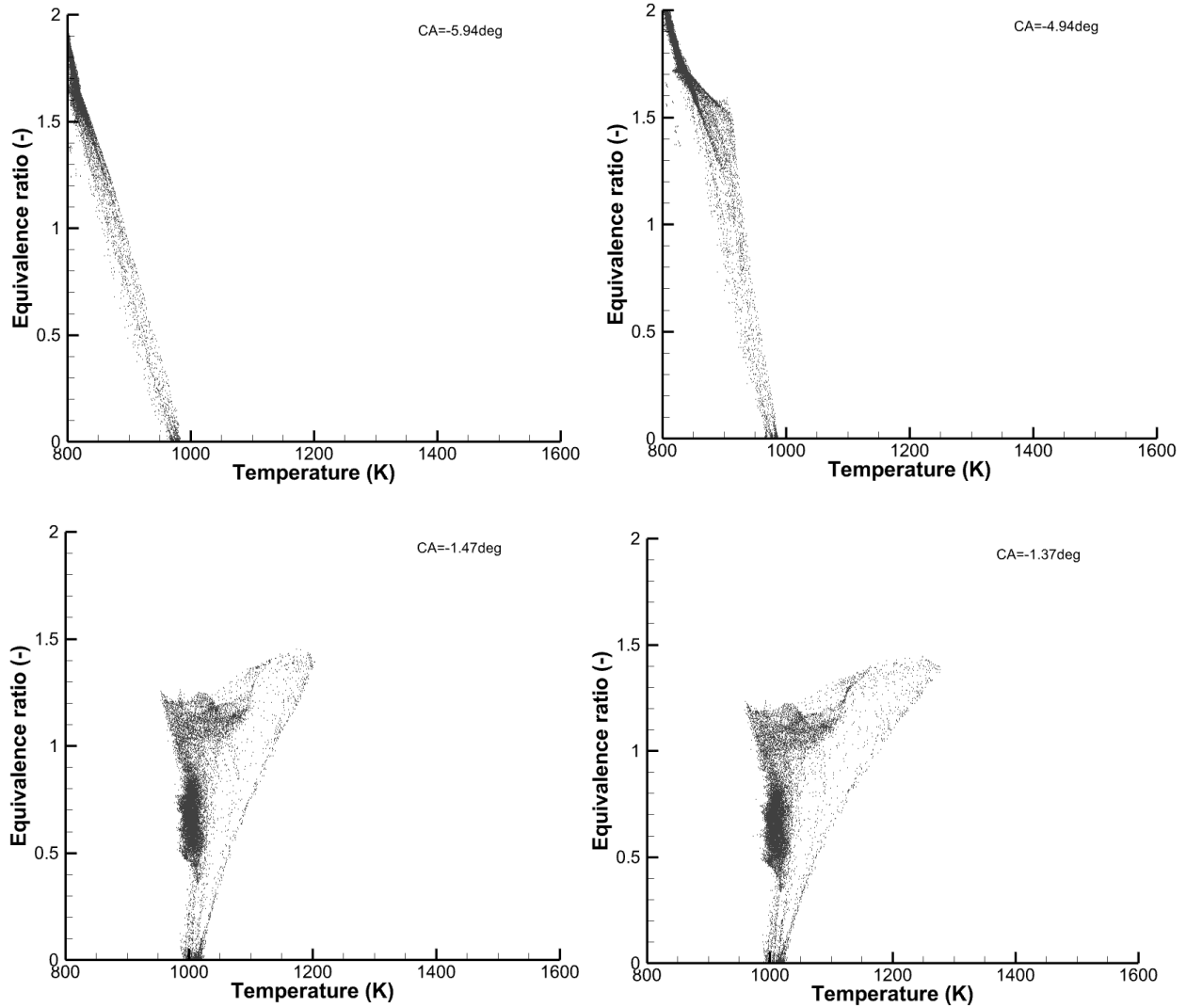


Figure 12: Phase scatter plots of equivalence ratio and gas temperature at CA=-5.94, -4.94, -1.47, and -1.37 degrees for Case 1; SOI=-10 degrees ATDC. Ignition occurs at -1.37 ATDC.

Figure 12 shows the phase scatter plots of equivalence ratio and gas temperature at CA=-5.94, -4.94, -1.47, and -1.37 degrees for the case in Figure 11. Comparing to the plot at -5.94 degrees, some points with equivalence ratio around 1.5 shift toward higher temperature, which implies that local ignition driving mixture induced by the low-temperature chemistry around 900K. The heat release from the low-temperature combustion increases the temperature of the mixture up to 1200K, which in return accelerates the subsequent chemical reactions and chain branching. Meanwhile,

the equivalence ratio of the cloud starts to drop due to mixing. Eventually, thermal runaway occurs in the mixture with equivalence ratio of 1.4 at CA=-1.47 degrees in the cylinder.

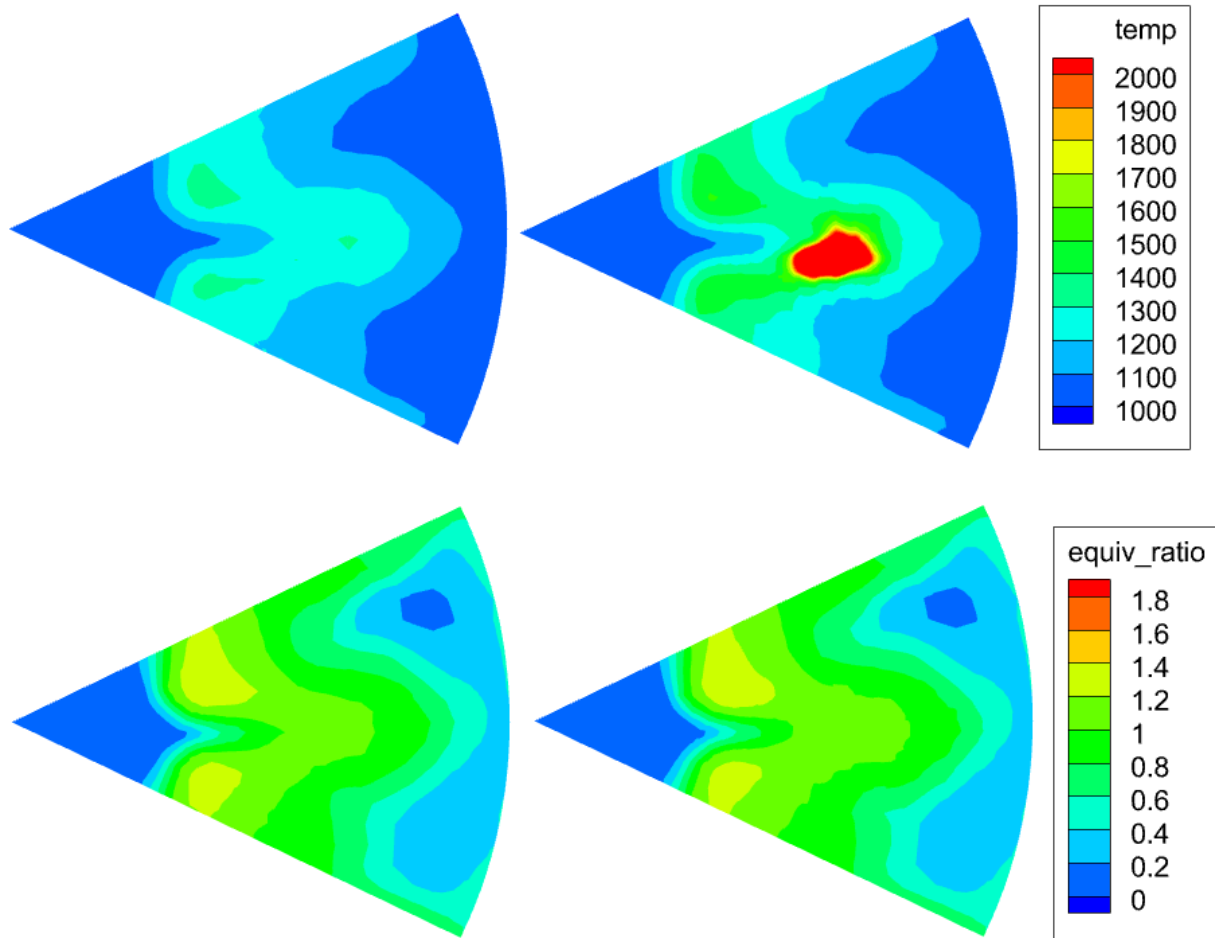


Figure 13: temperature (top) and equivalence ratio (botto) distribution before and after ignition (Case 3; SOI=-10 degrees ATDC): CA= 0.43 (left) and 0.52 (right) degrees ATDC.

Figure 13 shows the temperature and equivalence ratio distribution before (CA=0.43 degrees, ATDC, left) and after ignition (CA=0.52 degree ATDC, right) of Case 3 ($p_{boost} = 2 \text{ bar}$; $T_{boost} = 365 \text{ K}$; $\text{fuel sensitivity} = 9$) and SOI=-10 degrees ATDC. With higher fuel sensitivity, it shows greater stratification in temperature distribution than Case 1. This is primarily due to the higher toluene content and hence slower evaporation of higher fuel sensitivity fuel than PRF. The flame

also shows a W-shape in top view. It implies that the fuel injection, injection-induced charge motion, and fuel/air mixing are similar with different fuel sensitivity. Similar distributions of temperature and equivalence ratio as Case 1 are observed. This analysis further shows the PPCI-like combustion for beyond RON conditions, and indicates that the effect from chemical kinetics is stronger than those from thermodynamics and fluid dynamics with varying octane sensitivity.

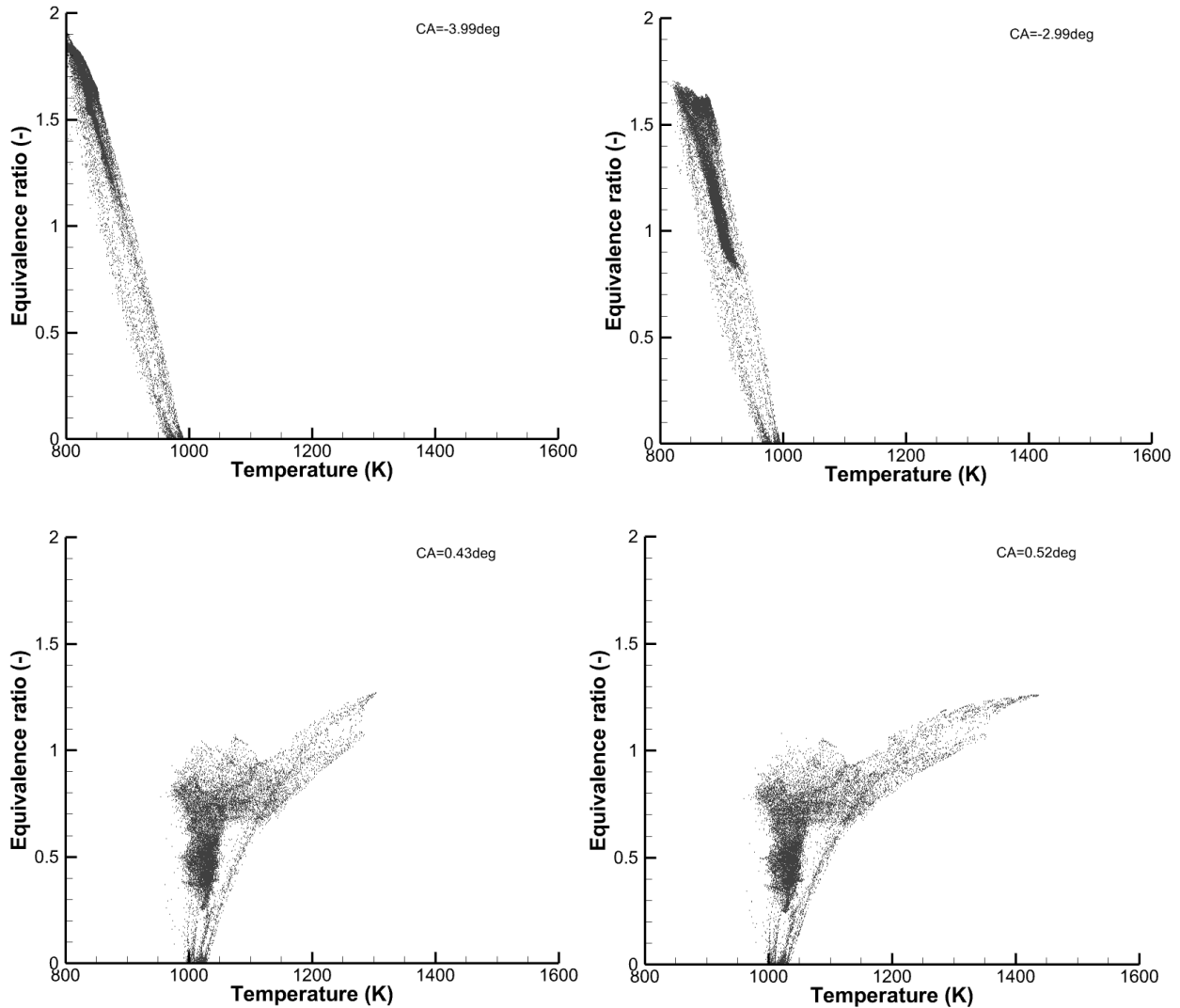


Figure 14: Phase scatter plots of equivalence ratio and gas temperature at CA=-3.99, -2.99, 0.43, and 0.52 degrees (Case 3; SOI=-10 degrees ATDC).

Figure 14 shows the phase scatter plots of equivalence ratio and gas temperature at CA=-3.99, -2.99, 0.43, and 0.52 degrees of Case 3 with SOI of -10 degree ATDC. At CA=-2.99 degrees, some

phase points with very rich equivalence ratio and low temperature shift to higher temperature, leaner space. With the progress of the chemical reactions and mixing, heat release from the mixture around stoichiometric (equivalence ratio is about 0.8~1.3) is observed. Particularly at CA=0.43 degrees, the mixture with equivalence ratio of 1.26 has the highest temperature around 1300K that eventually leads to auto-ignition. Results in Figure 11-Figure 14 then shows typical PPCI combustion mode for late injection under beyond RON conditions.

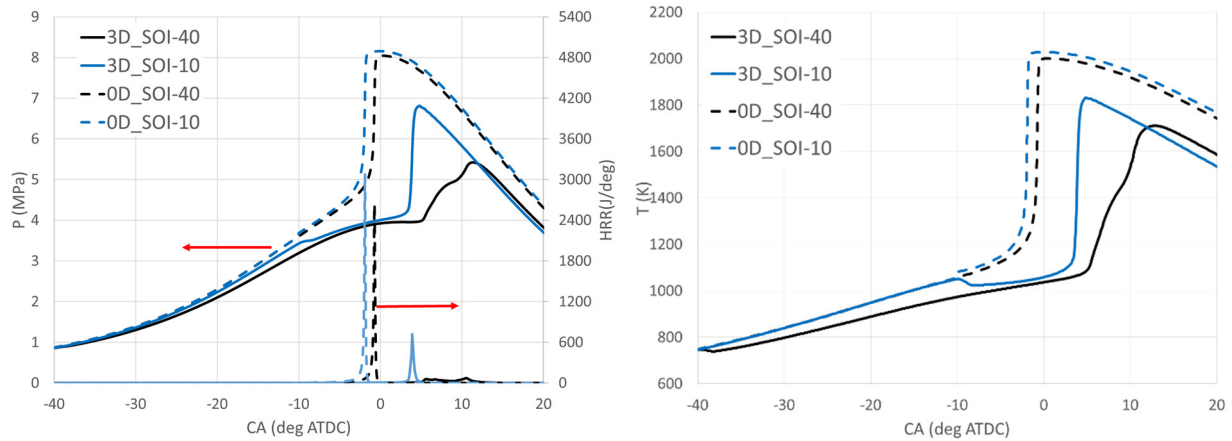


Figure 15: comparisons of pressure trace and heat release rate (left), and averaged in-cylinder temperature (right) between 0D and 3D CFD simulations (Case 4: $p_{boost} = 1 \text{ bar}$; $T_{boost} = 415 \text{ K}$; $S=0$).

Figure 15 shows the comparisons of pressure trace and heat release rate (left), and averaged in-cylinder temperature (right) between 0D and 3D CFD simulations of Case 4 ($p_{boost} = 1 \text{ bar}$; $T_{boost} = 415 \text{ K}$; $S=0$) with different injection timing. Cooling effects are evident by comparing the 0D and 3D results. Due to larger temperature difference between the liquid phase and gas phase, the cooling effects in the beyond-MON cases are more evident than those in the beyond-RON cases. Different from the beyond-RON cases, no heat release is observed in 3D

simulations of this case before TDC. It implies that the cooling effects reduce the charge temperature to a certain level that has prevented evident chemical reactions to occur. Considering that the current pressure is much lower than the other cases, the corresponding ignition delay is longer. Thus, the mixture is more sensitive to the temperature. The cooling effects become more dominant during the ignition processes. Eventually it causes significant delay in combustion phasing for Cases 4-6.

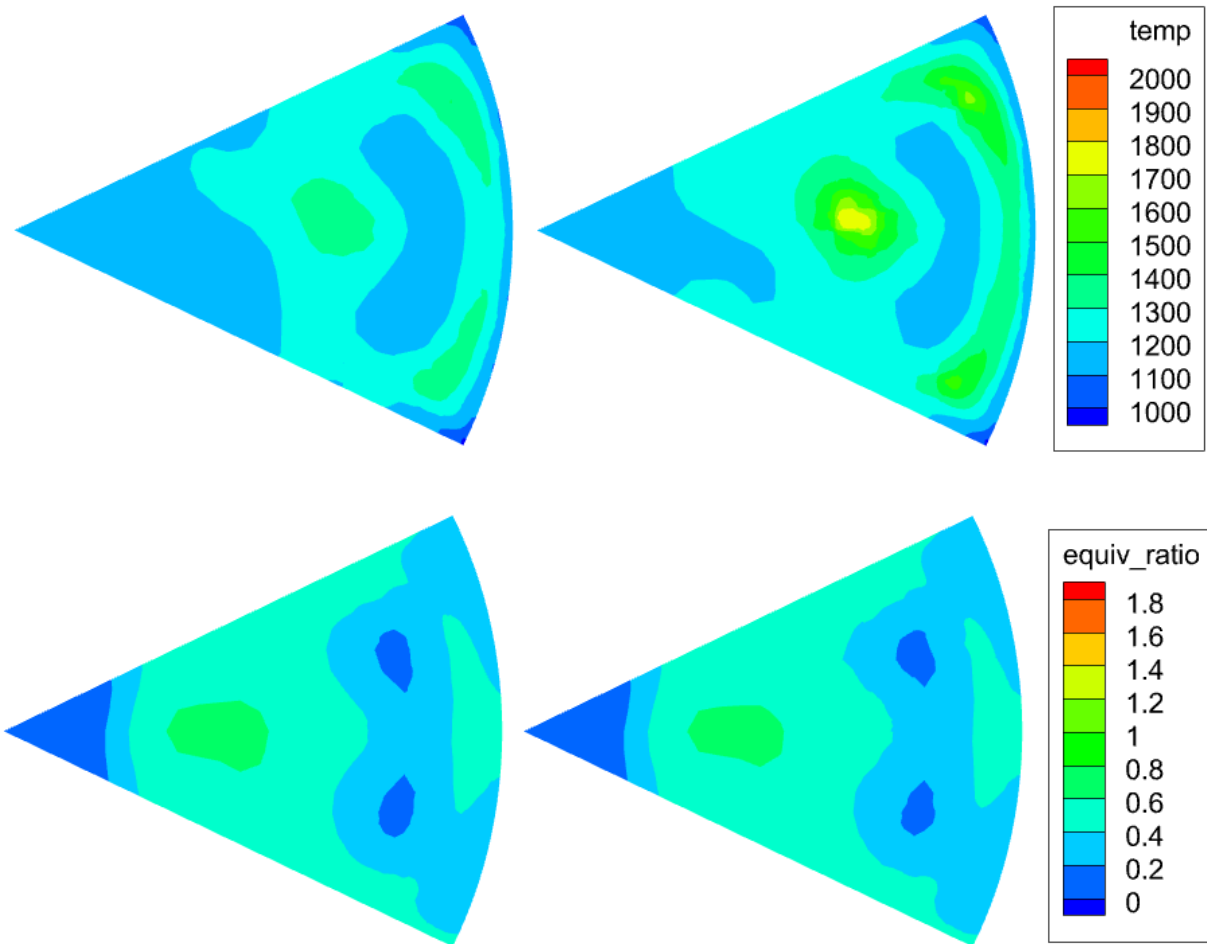
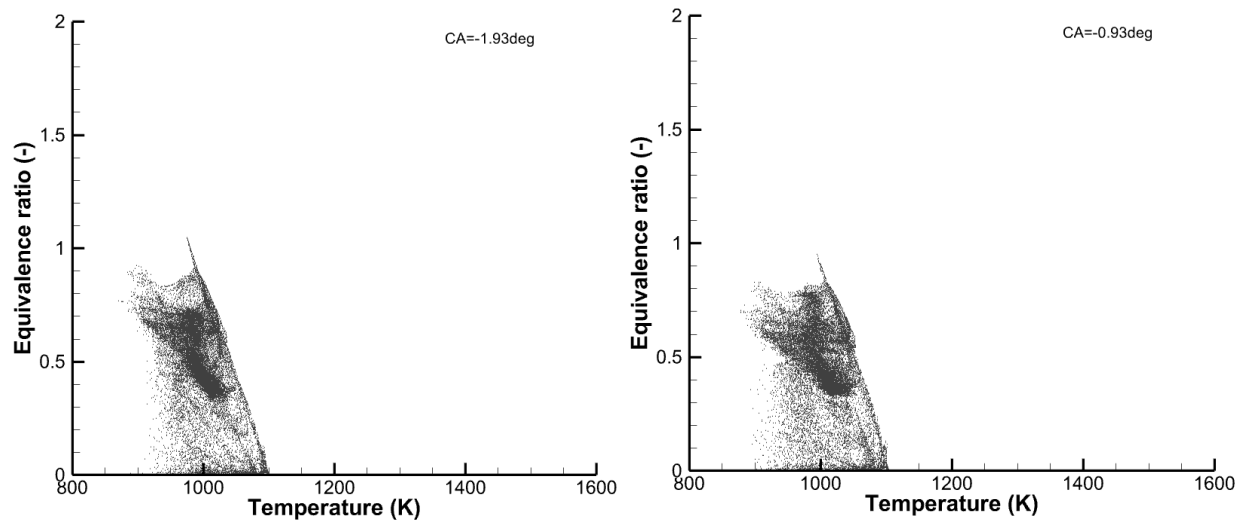


Figure 16: Temperature (top) and equivalence ratio (bottom) distribution before and after ignition (Case 4: $p_{boost} = 1 \text{ bar}$; $T_{boost} = 415 \text{ K}$; $S = 0$; SOI=-10 degrees ATDC): CA=3.44 and 3.53 degrees ATDC.

Figure 16 shows the temperature and equivalence ratio distribution before and after ignition of the beyond-MON Case 4 ($p_{boost} = 1 \text{ bar}$; $T_{boost} = 415 \text{ K}$; $S = 0$) and SOI=-10 degrees ATDC. The

top row is temperature. The bottom row is equivalence ratio. For each row, the left column implies the instant before ignition (3.44 ATDC) while the right column is after ignition (3.53 ATDC) respectively. Unlike the W-shape scalar distribution, the temperature and equivalence ratio distributions before ignition are much more homogeneous compared to the ones of the beyond- RON cases with the same injection timing. This is due to the stronger cooling effects for the beyond- MON cases that leads to longer ignition delay. Consequently, the charge has longer time for mixing that significantly reduces the stratification level. The local ignition driving mixtures have equivalence ratio of 0.4~0.6, which is much lower than the beyond- RON cases. The W-shape distribution in temperature or equivalence ratio is not observed in this case, as the momentum from the spray injection largely decays. Multiple ignition spots are observed near the wall and in the middle of cylinder center and wall, which implies that the present combustion is closer to a HCCI-type combustion.



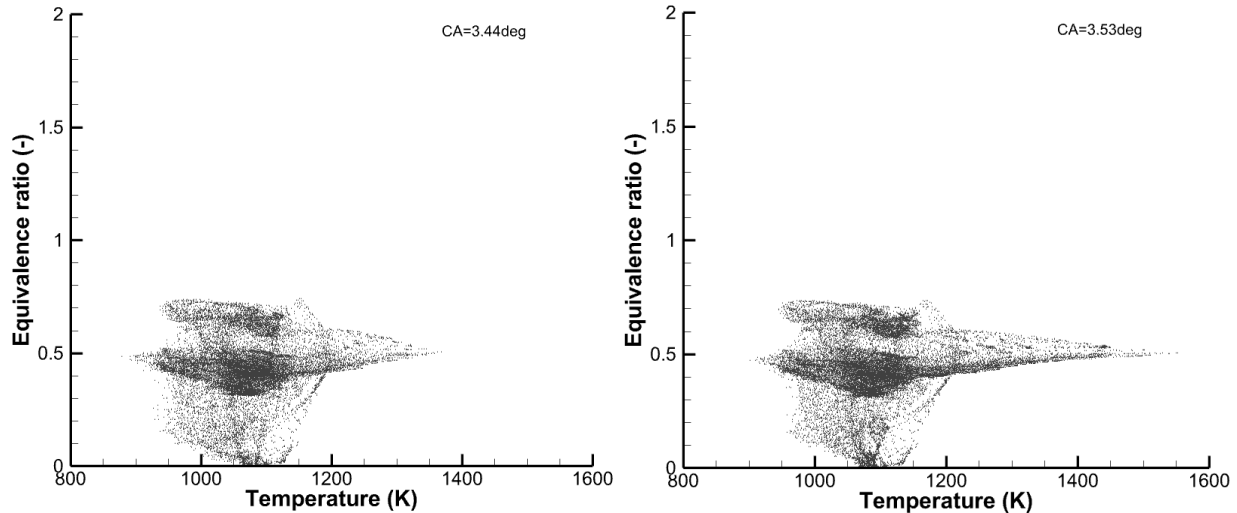


Figure 17: Phase scatter plots of equivalence ratio and gas temperature at CA=-1.93, -0.93, 3.44, and 3.53 degrees (Case 4; SOI=-10 degrees ATDC).

Figure 17 shows the phase scatter plots of equivalence ratio and gas temperature at CA=-1.93, -0.93, 3.44, and 3.53 degrees of Case 4 with SOI of -10 degree ATDC. During the ignition process, there is no rich mixture in the combustion chamber. The maximum equivalence ratio is about 1. This much narrower range of equivalence ratio directly suggests the much weaker degrees of stratifications. At CA=3.44 degrees ATDC, ignition occurs in the mixture with equivalence ratio of 0.4~0.6 and drives the temperature to around 1400K. The weaker stratification and occurrence of multiple hot spots fundamentally emphasizes the feature of HCCI-like combustion under beyond MON conditions. In all the investigated cases, the liquid fuel has completely vaporized before the ignition event. The combustion events are mainly PCCI- or HCCI-type combustion. This is due to the low overall equivalence ratio (0.3). A separated study with overall equivalence ratio of 0.6 showed that the liquid droplets exist when auto-ignition occurs. Thus, MCCI-type combustion can be expected under higher load conditions.

4. Conclusions

In the present paper, 0D and 3D combustion CFD simulations are employed to investigate the combustion processes of a gasoline direct injection compression ignition engine. Different surrogate fuel models with same RON and different fuel sensitivity are considered. The same reaction mechanism is used in both 0D and 3D simulations. ConvergeTM was used for the 3D combustion simulations, while ANSYS Chemkin-Pro for 0D simulations. The effects of fuel sensitivity and RON on combustion phasing are investigated. For 3D combustion simulation, the effects of injection timing are also studied. Comparing to 0D simulations that only consider the effects of thermodynamic condition and chemical kinetics, the 3D simulations consider additional effects of liquid fuel evaporation and mixing. The results of 0D and 3D simulations are compared to understand the impacts of individual factors. The following conclusions can be drawn:

- (1) The differences between 0D and 3D simulation results are due to the cooling effects from evaporation and stratifications in temperature and equivalence ratio distribution. Stratification in temperature is relatively less evident than the stratification in equivalence ratio. Stratifications in equivalence ratio will decrease ignition delay for present lean operations, while cooling effects could lead to different consequences depending on whether the operating condition is within NTC regime or not.
- (2) With typical beyond-RON operating condition with high boost pressure and low boost temperature, stratification effects are more dominant that can lead to shorter ignition delay in 3D simulation than 0D simulations. With typical beyond-MON conditions, cooling effects reduces the charge temperature to certain level that prevents exothermic chemical reactions occur and leads to longer ignition delay.
- (3) Early injection creates more homogeneous charge before the ignition than the late injection. Ignition delay that indicated by CA0_10 decreases with retarded injection timing due to

higher in-cylinder pressure and temperature. The higher in-cylinder temperature enhances evaporation process, while the higher in-cylinder density enhances droplet breakup process, both of which contribute to shorter ignition delay.

(4) For beyond-RON cases, the ignition driving mixture is found to be rich (1.4 ~ 1.6) and the in-cylinder charge is strongly stratified with W-shape distribution. The GDCI combustion mode is fundamentally PPCI-like combustion.

(5) For beyond-MON cases, the ignition driving mixture is found to be lean (0.4 ~ 0.6) and the in-cylinder charge is weakly stratified without the W-shape distribution. The GDCI combustion mode is fundamentally HCCI-like combustion.

(6) Higher fuel sensitivity leads to slower evaporation, because of the higher volatility of iso-octane comparing to toluene. Slower evaporation slows down mixing process. Thus, it increases the stratifications, and extends the cooling period. For the current conditions, ignition occurs after the liquid fuel completely vaporizes, and the difference in evaporation has negligible impact on the combustion.

Acknowledgement:

The authors acknowledge the support of Convergent Science Inc. to this research by providing the free academic license. The authors acknowledge the High-Performance Computing Center (HPCC) at Texas Tech University at Lubbock for providing HPC resources that have contributed to the research results reported within this paper. PZ is partially supported by the Co-Optimization of Fuels and Engines (Co-Optima) initiative sponsored by the US Department of Energy Office of Energy Efficiency and Renewable Energy and Bioenergy Technologies and Vehicle Technologies Offices, with Award Number DE-EE0007985.

References:

1. Reitz RD. Directions in internal combustion engine research. *Combustion and Flame*, 2013; 160: 1-8. DOI: <https://doi.org/10.1016/j.combustflame.2012.11.002>.
2. Kalghatgi GT, Risberg P and Ångström H-E. Advantages of fuels with high resistance to auto-ignition in late-injection, low-temperature, compression ignition combustion. *SAE Transactions*, 2006: 623-634. DOI: <https://doi.org/10.4271/2006-01-3385>.
3. Kalghatgi GT, Risberg P and Ångström H-E. Partially pre-mixed auto-ignition of gasoline to attain low smoke and low NO_x at high load in a compression ignition engine and comparison with a diesel fuel. *SAE Technical paper 2007-01-0006*, 2007. DOI: <https://doi.org/10.4271/2007-01-0006>.
4. Sellnau M, Foster M, Hoyer K, et al. Development of a gasoline direct injection compression ignition (GDCI) engine. *SAE International Journal of Engines*, 2014; 7: 835-851. DOI: <https://doi.org/10.4271/2014-01-1300>.
5. Sellnau M, Foster M, Moore W, et al. Second generation GDCI multi-cylinder engine for high fuel efficiency and US tier 3 emissions. *SAE International Journal of Engines*, 2016; 9: 1002-1020. DOI: <https://doi.org/10.4271/2016-01-0760>.
6. Sellnau M, Moore W, Sinnamon J, et al. GDCI multi-cylinder engine for high fuel efficiency and low emissions. *SAE international journal of engines*, 2015; 8: 775-790. DOI: <https://doi.org/10.4271/2015-01-0834>.
7. Sellnau M, Sinnamon J, Hoyer K, et al. Gasoline direct injection compression ignition (GDCI)-diesel-like efficiency with low CO₂ emissions. *SAE International Journal of Engines*, 2011; 4: 2010-2022. DOI: <https://doi.org/10.4271/2011-01-1386>.
8. Sellnau MC, Sinnamon J, Hoyer K, et al. Full-time gasoline direct-injection compression ignition (GDCI) for high efficiency and low NO_x and PM. *SAE International Journal of Engines*, 2012; 5: 300-314. DOI: <https://doi.org/10.4271/2012-01-0384>.
9. Sellnau MC, Sinnamon J, Hoyer K, et al. Part-load operation of gasoline direct-injection compression ignition (GDCI) engine. *SAE Technical Paper 2013-01-0272*, 2013. DOI: <https://doi.org/10.4271/2013-01-0272>.

10. Sellnau M, Hoyer K, Moore W, et al. Advancement of GDCI engine technology for US 2025 CAFE and Tier 3 emissions. *SAE Technical Paper 2018-01-0901*, 2018. DOI: <https://doi.org/10.4271/2018-01-0901>.
11. Sellnau M, Hoyer K, Petot JH, et al. Fuel Injection System for Opposed-Piston Gasoline Compression-Ignited (OP-GCI) Engines. *SAE Technical Paper 2019-01-0287*, 2019. DOI: <https://doi.org/10.4271/2019-01-0287>.
12. Badra J, Bakor R, AlRamadan A, et al. Standardized Gasoline Compression Ignition Fuels Matrix. *SAE Technical Paper 2018-01-0925*, 2018. DOI: <https://doi.org/10.4271/2018-01-0925>.
13. Badra J, Zubail A and Sim J. Numerical Investigation into Effects of Fuel Physical Properties on GCI Engine Performance and Emissions. *Energy & Fuels*, 2019; 33: 10267-10281. DOI: <https://doi.org/10.1021/acs.energyfuels.9b02340>.
14. Badra JA, Sim J, Viollet Y, et al. CFD Guided Gasoline Compression Ignition Engine Calibration. In: *ASME 2017 Internal Combustion Engine Division Fall Technical Conference 2017*, pp.ICEF2017-3583. American Society of Mechanical Engineers Digital Collection.
15. Zhang Y, Pei Y, Engineer N, et al. CFD-Guided Combustion Strategy Development for a Higher Reactivity Gasoline in a Light-Duty Gasoline Compression Ignition Engine. *SAE Technical Paper 2017-01-0740*, 2017. DOI: <https://doi.org/10.4271/2017-01-0740>.
16. Zhang Y, Kumar P, Pei Y, et al. An Experimental and Computational Investigation of Gasoline Compression Ignition Using Conventional and Higher Reactivity Gasolines in a Multi-Cylinder Heavy-Duty Diesel Engine. *SAE Technical Paper 2018-01-0226*, 2018. DOI: <https://doi.org/10.4271/2018-01-0226>.
17. Cho K, Zhang Y and Cleary D. Investigation of Fuel Effects on Combustion Characteristics of Partially Premixed Compression Ignition (PPCI) Combustion Mode at Part-Load Operations. *SAE Technical Paper 2018-01-0897*, 2018. DOI: <https://doi.org/10.4271/2018-01-0897>.
18. Ra Y, Yun JE and Reitz RD. Numerical parametric study of diesel engine operation with gasoline. *Combustion Science and Technology*, 2009; 181: 350-378. DOI: <https://doi.org/10.1080/00102200802504665>.
19. Ra Y, Loeper P, Reitz R, et al. Study of high speed gasoline direct injection compression ignition (GDICI) engine operation in the LTC regime. *SAE International Journal of Engines*, 2011; 4: 1412-1430. DOI: <https://doi.org/10.4271/2011-01-1182>.

20. Adhikary BD, Ra Y, Reitz RD, et al. Numerical optimization of a light-duty compression ignition engine fuelled with low-octane gasoline. *SAE Technical Paper 2012-01-1336*, 2012. DOI: <https://doi.org/10.4271/2012-01-1336>.
21. Adhikary BD, Reitz RD, Ciatti S, et al. Computational investigation of low load operation in a light-duty gasoline direct injection compression ignition [GDICI] engine using single-injection strategy. *SAE Technical Paper 2014-01-1297*, 2014. DOI: <https://doi.org/10.4271/2014-01-1297>.
22. Roberts J, Kokjohn S, Hou D, et al. Performance of Gasoline Compression Ignition (GCI) with On-Demand Reactivity Enhancement over Simulated Drive Cycles. *SAE Technical Paper 2018-01-0255*, 2018. DOI: <https://doi.org/10.4271/2018-01-0255>.
23. Manente V, Johansson B and Tunestal P. Partially premixed combustion at high load using gasoline and ethanol, a comparison with diesel. *SAE Technical Paper 2009-01-0944*, 2009. DOI: <https://doi.org/10.4271/2009-01-0944>.
24. Manente V, Johansson B, Tunestal P, et al. Effects of different type of gasoline fuels on heavy duty partially premixed combustion. *SAE International Journal of Engines*, 2010; 2: 71-88. DOI: <https://doi.org/10.4271/2009-01-2668>.
25. Manente V, Tunestal P, Johansson B, et al. Effects of ethanol and different type of gasoline fuels on partially premixed combustion from low to high load. *SAE Technical Paper 2010-01-0871*, 2010. DOI: <https://doi.org/10.4271/2010-01-0871>.
26. Manente V, Zander C-G, Johansson B, et al. An advanced internal combustion engine concept for low emissions and high efficiency from idle to max load using gasoline partially premixed combustion. *SAE Technical Paper 2010-01-2198*, 2010. DOI: <https://doi.org/10.4271/2010-01-2198>.
27. Hildingsson L, Kalghatgi G, Tait N, et al. Fuel octane effects in the partially premixed combustion regime in compression ignition engines. *SAE Technical Paper 2009-01-2648*, 2009. DOI: <https://doi.org/10.4271/2009-01-2648>.
28. Borgqvist P, Tunestal P and Johansson B. Comparison of negative valve overlap (NVO) and rebreathing valve strategies on a gasoline PPC engine at low load and idle operating conditions. *SAE International Journal of Engines*, 2013; 6: 366-378. DOI: <https://doi.org/10.4271/2013-01-0902>.

29. Kodavasal J, Kolodziej CP, Ciatti SA, et al. Computational Fluid Dynamics Simulation of Gasoline Compression Ignition. *Journal of Energy Resources Technology*, 2015; 137. DOI: 10.1115/1.4029963.
30. Cung K and Ciatti S. A study of injection strategy to achieve high load points for gasoline compression ignition (GCI) operation. In: *ASME 2017 Internal Combustion Engine Division Fall Technical Conference 2017*, pp.ICEF2017-3625. American Society of Mechanical Engineers Digital Collection.
31. Cung KD, Ciatti SA, Tanov S, et al. low-Temperature combustion of high Octane Fuels in a gasoline compression ignition engine. *Frontiers in Mechanical Engineering*, 2017; 3: 22. DOI: 10.3389/fmech.2017.00022.
32. Wang B, Pamminger M, Vojtech R, et al. Impact of injection strategies on combustion characteristics, efficiency and emissions of gasoline compression ignition operation in a heavy-duty multi-cylinder engine. *International Journal of Engine Research*, 2018: 1468087418801660.
33. Kodavasal J, Kolodziej CP, Ciatti SA, et al. Effects of injection parameters, boost, and swirl ratio on gasoline compression ignition operation at idle and low-load conditions. *International Journal of Engine Research*, 2017; 18: 824-836.
34. Woo C, Goyal H, Kook S, et al. Double injection strategies for ethanol-fuelled Gasoline compression ignition (GCI) combustion in a single-cylinder light-duty diesel engine. *SAE Technical Paper 2016-01-2303*, 2016. DOI: <https://doi.org/10.4271/2016-01-2303>.
35. Goyal H and Kook S. Ignition process of gasoline compression ignition (GCI) combustion in a small-bore optical engine. *Fuel*, 2019; 256: 115844.
36. Goyal H, Kook S, Hawkes E, et al. Influence of Engine Speed on Gasoline Compression Ignition (GCI) Combustion in a Single-Cylinder Light-Duty Diesel Engine. *SAE Technical Paper 2017-01-0742*, 2017. DOI: <https://doi.org/10.4271/2017-01-0742>.
37. Goyal H, Kook S and Ikeda Y. The influence of fuel ignition quality and first injection proportion on gasoline compression ignition (GCI) combustion in a small-bore engine. *Fuel*, 2019; 235: 1207-1215.
38. Kalghatgi G and Johansson B. Gasoline compression ignition approach to efficient, clean and affordable future engines. *Proceedings of the Institution of Mechanical Engineers, Part D: Journal of Automobile Engineering*, 2018; 232: 118-138.

39. Dempsey AB, Curran S, Wagner R, et al. Gasoline Compression Ignition on a Light-Duty Multi-Cylinder Engine Using a Wide Range of Fuel Reactivities and Heavy Fuel Stratification. *Journal of Energy Resources Technology*, 2021; 143. DOI: 10.1115/1.4050742.
40. Tao M, Zhao P, DelVescovo D, et al. Manifestation of octane rating, fuel sensitivity, and composition effects for gasoline surrogates under advanced compression ignition conditions. *Combustion and Flame*, 2018; 192: 238-249. DOI: <https://doi.org/10.1016/j.combustflame.2018.02.015>.
41. Tao M, Wu T, Ge H, et al. A kinetic modeling study on octane rating and fuel sensitivity in advanced compression ignition engines. *Combustion and Flame*, 2017; 185: 234-244. DOI: <https://doi.org/10.1016/j.combustflame.2017.07.020>.
42. Messerly RA, Luecke JH, St. John PC, et al. Understanding how chemical structure affects ignition-delay-time ϕ -sensitivity. *Combustion and Flame*, 2021; 225: 377-387. DOI: <https://doi.org/10.1016/j.combustflame.2020.11.004>.
43. Lopez Pintor D, Dec J and Gentz G. Φ -Sensitivity for LTGC Engines: Understanding the Fundamentals and Tailoring Fuel Blends to Maximize This Property. *SAE Technical Paper 2019-01-0961*, 2019. DOI: <https://doi.org/10.4271/2019-01-0961>.
44. Szybist JP, Wagnon SW, Splitter D, et al. The Reduced Effectiveness of EGR to Mitigate Knock at High Loads in Boosted SI Engines. *SAE International Journal of Engines*, 2017; 10: 2305-2318.
45. Tao M, Zhao P, Szybist JP, et al. Insights into engine autoignition: Combining engine thermodynamic trajectory and fuel ignition delay iso-contour. *Combustion and Flame*, 2019; 200: 207-218. DOI: <https://doi.org/10.1016/j.combustflame.2018.11.025>.
46. Ge HW, Shi Y, Reitz RD, et al. Optimization of a HSDI diesel engine for passenger cars using a multi-objective genetic algorithm and multi-dimensional modeling. *SAE International Journal of Engines*, 2009; 2: 691-713. DOI: 10.4271/2009-01-0715.
47. Richards K, Senecal P and Pomraning E. *CONVERGE 2.4 Manual*. 2017. Madison, WI: Convergent Science, Inc.
48. Ge HW and Cho N. Effects of Numerical Models on Prediction of Cylinder Pressure Ringing in a DI Diesel Engine. *SAE Technical Paper 2018-01-0194*, 2018. DOI: <https://doi.org/10.4271/2018-01-0194>.

49. Han Z and Reitz RD. Turbulence Modeling of Internal Combustion Engines Using RNG κ - ϵ Models. *Combustion Science and Technology*, 1995; 106: 267-295. DOI: 10.1080/00102209508907782.
50. Beale JC and Reitz RD. Modeling spray atomization with the Kelvin-Helmholtz/Rayleigh-Taylor hybrid model. *Atomization and Sprays*, 1999; 9. DOI: 10.1615/AtomizSpr.v9.i6.40.
51. O'Rourke P and Amsden A. *Three dimensional numerical simulations of the UPS-292-SC engine*. 1987. Los Alamos National Lab., NM (USA).
52. Frossling N. Uber die verdunstung fallender tropfen. *Gerlands Beitrage zur Geophysik*, 1938; 52: 170-216.
53. Kalghatgi G, Babiker H and Badra J. A Simple Method to Predict Knock Using Toluene, N-Heptane and Iso-Octane Blends (TPRF) as Gasoline Surrogates. *SAE International Journal of Engines*, 2015; 8: 505-519. DOI: <https://doi.org/10.4271/2015-01-0757>.
54. Andrae JCG. Comprehensive chemical kinetic modeling of toluene reference fuels oxidation. *Fuel*, 2013; 107: 740-748. DOI: <https://doi.org/10.1016/j.fuel.2013.01.070>.
55. Xiao G, Ge H and Zhao P. Initiation and propagation of one-dimensional planar flames in mixtures with variable reaction progress. *Combustion and Flame*, 2022; 236: 111765. DOI: <https://doi.org/10.1016/j.combustflame.2021.111765>.
56. Hwang J, Weiss L, Karathanassis IK, et al. Spatio-temporal identification of plume dynamics by 3D computed tomography using engine combustion network spray G injector and various fuels. *Fuel*, 2020; 280: 118359. DOI: <https://doi.org/10.1016/j.fuel.2020.118359>.
57. Leppard WR. The Chemical Origin of Fuel Octane Sensitivity. *SAE Transactions*, 1990; 99: 862-876. DOI: <https://doi.org/10.4271/902137>.